MOLECULAR DYNAMICS SIMULATIONS OF POLYMER SYSTEMS

BURKHARD DÜNWEG*, GARY S. GREST†, and KURT KREMER*

Abstract

A brief general introduction into Molecular Dynamics methods for polymers is given. For the statics and dynamics of an isolated chain, a simple microcanonical algorithm is severely hampered by ergodicity problems due to mode conservation. Coupling the system to a Langevin heat bath solves this problem, but also screens hydrodynamic interactions for a chain in a bath of solvent molecules. Rouse scaling laws should hold whenever long–range interactions and entanglements are not important; this is important for controlling the relevant time scales as well as for checking the correctness of simulation algorithms. As an application, a single chain in a bath of solvent particles is discussed. In this system, the long–range nature of the hydrodynamic interaction induces pronounced finite size effects, which are analyzed using Ewald summation methods. Furthermore, simulations on the dynamics of entangled melts are considered. Starting from the reptation picture, we discuss the difficulties to observe this behavior, even with state–of–the–art hardware and simulation methods. New and improved data on long runs of melts of chains of up to 350 monomers are presented.

Keywords

Molecular Dynamics, Stochastic Dynamics, Polymer Dynamics, Rouse Model, Zimm Model, Hydrodynamic Interaction, Reptation Model

*Max Planck–Institut für Polymerforschung, Ackermannweg 10, D–55128 Mainz, Germany

†Corporate Research Science Laboratory, Exxon Research and Engineering Company, Annandale, NJ 08801, USA

1 Introduction

Computer simulations in polymer science pursue a two–fold goal. The first is to understand (and, as a long–term goal, even reliably predict) the properties of real materials like polyethylene, based on the details of the chemical structure. Secondly, there are still a number of unsolved questions which are not related to specific materials, but rather of a quite general and fundamental nature, and whose solution is, to our minds, indispensable for real progress in our ability to predict material properties. While there has been considerable progress in understanding some aspects of polymer behavior using universal scaling laws [1], there remain many unresolved problems. To mention just a few examples: The structure of polyelectrolyte solutions as a function of fundamental parameters like concentration, chain length, and charge density, is only understood in limiting cases. Similarly, the viscoelastic behavior of neutral polymer melts is still under debate: While the reptation model [2] provides a very useful and simple picture about the microscopic and macroscopic consequences of the impossibility of chains crossing each other, its predictions are only partly in agreement with experimental findings — most famous is the prediction for the viscosity to scale with the third power of the chain length, while experiments find an exponent of 3.4. Another example is the dynamics of polymer solutions. There is no clear explanation why the hydrodynamic interaction, which governs the behavior in the dilute limit, is completely screened at higher concentrations, although the solution as a whole is of course still a viscous fluid with hydrodynamic fluctuations [2].

Computer simulations can make very useful contributions to questions like these, since they can study very *simple* well–defined model systems (with many of the experimental difficulties removed) in considerable detail. The main advantage is that all degrees of freedom are known explicitly, such that questions of microscopic structure and mechanisms of motion can be answered, while experiments often have only limited and indirect access to the pertinent quantities. For example, in a simulation it is very easy to measure the hydrodynamic radius of a chain as a *static* quantity, while light scattering experiments can only measure it indirectly as a *dynamic* quantity. In polymer melts, neutron scattering experiments allow only indirect conclusions about the possible dominance of curvilinear motion, while in a simulation this can be seen directly. Of course, there are strong limitations with respect to both system size and (even more severely) observation time, since the relaxation time increases very

strongly with chain length.

In general, there are two types of computer simulation algorithms, Molecular Dynamics (MD), based on the solution of Newton's equation of motion, and Monte Carlo (MC), based on a Markov process in configuration space. There is no general answer to the question which method is "better"; to a large extent, this depends on the system under consideration, and, even more so, on the scientific question which one would like to answer. Some comments on this issue can be found at the end of Sec. 2.

Since we cannot cover all MD simulations which have been done on simple polymer models, we restrict ourselves to a brief summary of two large–scale simulations which have been done on the dynamics of dilute polymer solutions [3, 4] (Sec. 4) and dense melts [5, 6] (Sec. 5). In the latter case we mainly present new and improved data which have not yet been reported elsewhere. Prior to this in Secs. 2 and 3 we discuss the Rouse and Zimm model, respectively, with emphasis on the methodological implications for simulations.

For more information, we refer the reader to a recent collection of reviews [7] on polymer simulations, as well as to the proceedings of recent summer schools on computer simulations in general [8, 9]. For more "technical" information on MD simulation methods see Refs. [10–12]. Apart from the cases already mentioned, MD simulations (partly in combination with MC) have been successfully applied to polyelectrolyte solutions [13–15], networks [16–21], tethered chains [22] as well as polymer blends and block copolymers [23]. An important field whose impact will increase in the future, due to the advent of modern parallel computers, is the method of non–equilibrium Molecular Dynamics (NEMD). For an overview, we refer the reader to the article by Hess in Ref. [8]. This method has been successfully applied to polymeric liquids both in the regime of dilute solutions [24, 25] as well as to entangled melts [26].

2 Rouse behavior and simulation algorithms

A valid algorithm for the simulation of the generic features of the stochastic Brownian motion of polymer chains should, in certain limiting cases, be able to reproduce the behavior predicted by the scaling laws of the *Rouse model* [2, 27]. This model starts from the description of the chain conformation as a self–similar random fractal described by a universal exponent ν [1]: For the end–to–end distance R and the gyration radius R_G ($\vec{R} = \vec{r}_N - \vec{r}_1$ for an N–monomer chain, while

$R_G^2 = (1/2)N^{-2}\sum_{ij}(\vec{r}_i - \vec{r}_j)^2)$ the scaling laws $\langle R^2\rangle \propto \langle R_G^2\rangle \propto N^{2\nu}$ hold, where $\nu = 1/2$ for a random walk and $\nu = 0.59$ for a self–avoiding walk in three spatial dimensions. The same scaling holds, of course, for the relation between monomer–monomer distances and the corresponding lengths along the chain. For this reason, the single–chain static structure factor

$$S(k) = N^{-1}\sum_{ij}\left\langle \exp(i\vec{k}\cdot\vec{r}_{ij})\right\rangle \tag{1}$$

satisfies the scaling relation $S(k) \propto k^{-1/\nu}$ in the wavenumber regime $R_G^{-1} \ll k \ll a^{-1}$, a being the segment length. The second ingredient of the model is the assignment of a friction constant ζ to the monomers, while the third assumption consists of *statistically independent* stochastic monomer moves $\vec{\rho}_i$ in a short time interval h, such that

$$\vec{r}_i(t+h) = \vec{r}_i(t) + \zeta^{-1}\vec{F}_i h + \vec{\rho}_i. \tag{2}$$

The force $\vec{F}_i$ on the ith monomer is a thermodynamic driving force to which in general also entropic effects contribute:

$$\vec{F}_i = -\frac{\partial}{\partial\vec{r}_i}U\left(\{\vec{r}_i\}\right) \tag{3}$$

where

$$P\left(\{\vec{r}_i\}\right) \propto \exp\left(-U\left(\{\vec{r}_i\}\right)/k_BT\right) \tag{4}$$

is the equilibrium distribution function of the chain conformations. Here it is assumed that the effective potential U contains only short–range interactions. The stochastic displacements satisfy the usual fluctuation–dissipation theorem

$$\langle\vec{\rho}_i\rangle = 0 \tag{5}$$

and

$$\langle\vec{\rho}_i \otimes \vec{\rho}_j\rangle = 2D_0 h\delta_{ij}\overleftrightarrow{1}, \tag{6}$$

where the monomeric diffusion constant D_0 is related to the friction constant via the Einstein relation $D_0 = k_BT/\zeta$.

On sufficiently long length and time scales, this model should provide a *universal* description of polymer dynamics as soon as one deals with short–range interactions, uncorrelated displacements, and flexible polymer chains. The usual "coarse–graining" procedure [1] unites several subsequent chemical units to an effective coarse–grained monomer, with an effective friction constant and an effective

interaction. If this is done well beyond the persistence length, the picture becomes rather simple: For a random walk, P becomes a Gaussian, and $\vec{F}_i$ is just the force resulting from entropic springs [1, 2]. In the case of a self–avoiding walk, excluded volume forces contribute too. Thus the long–wavelength, long–time properties of the original chain and the coarse–grained chain (which is, in essence, a bead–spring model) should coincide, and the non–universal parameters of the latter (bead size and bead friction) just define the microscopic length and time scales beyond which universal behavior sets in.

From the above equation of motion, Eqn. 2, one immediately finds for the center of mass of the chain, $\vec{R}_{CM} = N^{-1} \sum_i \vec{r}_i$,

$$\vec{R}_{CM}(t+h) = \vec{R}_{CM}(t) + N^{-1} \sum_i \vec{\rho}_i, \tag{7}$$

since the force contributions exactly cancel. This, however, means that the diffusion constant of the chain is simply a factor of N smaller than D_0:

$$D_{CM} = \frac{D_0}{N} \propto R_G^{-1/\nu}. \tag{8}$$

The longest relaxation time, the so–called Rouse time τ_R, is when the chain has diffused its own size, i. e. $D_{CM}\tau_R \propto R_G^2$ or

$$\tau_R \propto R_G^{2+1/\nu} \propto N^{1+2\nu}. \tag{9}$$

This consideration has yielded the dynamic exponent z of the Rouse model, $z = 2 + 1/\nu$ [2]. Explicitly, one has $\tau_R \propto R_G^4 \propto N^2$ ($z = 4$) in the random walk case, while $\tau_R \propto R_G^{3.69} \propto N^{2.18}$ ($z = 3.69$) in the good solvent regime. More generally, z connects relaxation times with the corresponding length scales. In particular, for time scales $\tau_0 \ll t \ll \tau_R$ (τ_0 being a microscopic time, which is roughly given by the time a monomer needs to feel its connectivity to its neighbors), the mean square displacement of a monomer behaves sub–diffusively,

$$g_1(t) = \langle (\vec{r}_i(t) - \vec{r}_i(0))^2 \rangle \propto t^{2/z} \tag{10}$$

(i. e. a $t^{1/2}$ behavior in the random walk case, and $t^{0.54}$ for self–avoiding walks), while for times $t \gg \tau_R$ the monomer of course moves with the overall diffusion of the chain. A similar result holds for the single–chain dynamic structure factor

$$S(k,t) = N^{-1} \sum_{ij} \left\langle \exp\left\{ i\vec{k} \cdot (\vec{r}_i(t) - \vec{r}_j(0)) \right\} \right\rangle, \tag{11}$$

which in the scaling regime $R_G^{-1} \ll k \ll a^{-1}$, $\tau_0 \ll t \ll \tau_R$ satisfies the scaling relation

$$S(k,t) = k^{-1/\nu} f(k^z t). \tag{12}$$

Physically, the Rouse model provides a good description of the dynamics for short–chain melts. In melts, the excluded volume interaction is completely screened [1], such that the random walk case $\nu = 1/2$ applies. This is the only case where the dynamics can be solved *exactly*[1] [27]. However, from a fundamental point of view, it remains unclear why the complicated many–body effects in a melt can be simply replaced by a homogeneous viscous background. In long–chain melts, entanglement effects become important, and the dynamics is expected to be described by the reptation model [2]. Similarly, in dilute solutions hydrodynamic effects become important, and the dynamics is described by the Zimm model [2, 28–30], which will be explained in more detail below.

However, apart from being of physical importance for real systems, the Rouse model also provides a well–defined test for simulation algorithms, which should reproduce the above scaling laws in case one simulates a single chain in "vacuum", using uncorrelated displacements. For the stochastic dynamics algorithm to be described below, this detailed test was done in Ref. [31], and similar analyses have also been done for lattice models which employ local Monte Carlo moves [32]. Without going into further detail, we just want to point out here that suitable lattice Monte Carlo models can be used for a valid description of polymer dynamics both in the Rouse as well as the reptation regime, and have quite successfully been applied to the dynamics of polymer melts [33–35].

Note, however, that in either case the correct reproduction of Rouse behavior is less trivial than one might expect at first glance. In the case of lattice models [32], simple "kink–jump" moves introduce an artificial conservation law which results in unphysical dynamical behavior. The walk is built up from elementary steps $\vec{l}_i$, such that the end–to–end vector is $\vec{R} = \sum_i \vec{l}_i$. A kink–jump move in the inner part of the chain simply exchanges two subsequent steps $\vec{l}_i$ and $\vec{l}_{i+1}$, such that the set of bond vectors $\left\{\vec{l}_i\right\}$ remains unchanged. This conservation law, combined with the excluded–volume constraint, prevents, in essence, the annihilation of kink–antikink pairs, which can hence only be removed via diffusion out of the chain. Therefore, a reptation–like

[1] Often the term "Rouse model" is only used for this special case. However, we use it here more generally to denote a dynamic universality class.

scaling $\tau \propto N^3$ (see Sec. 5) results, which is of course unphysical for single–chain systems [32, 36]. It turns out that the inclusion of 90° "crankshaft" moves (on the three–dimensional simple cubic lattice) is sufficient to relax the chain in a Rouse–like way [32], since this destroys the conservation of the set of bond vectors $\left\{\vec{l}_i\right\}$.

Similarly, for the continuum Molecular Dynamics, a single–chain simulation quickly runs into problems of ergodicity, very similar to those which were found by Fermi, Pasta, and Ulam in the pioneering days of computer simulations [10]. The reason for this is that any model for a flexible polymer chain can, by coarse–graining, be mapped onto a bead–spring model (if it is not one already). Such a Hamiltonian is in turn very close to a *harmonic* system. Harmonic systems not only exhibit simple energy and momentum conservation, but rather the amplitude of every single normal mode is separately conserved. This means that the phase–space trajectory, instead of scanning the whole energy hypersurface, only visits a small subset of states such that time averages differ from microcanonical ensemble averages. For a weakly anharmonic system, the conservation laws of course no longer hold exactly. Nevertheless the mode amplitudes decorrelate only very slowly, such that one needs extremely long runs to obtain reasonable sampling properties. Of course, all these considerations do not hold for dense many–chain melts [5, 6], or a single chain surrounded by solvent particles [3, 4, 37, 38]. In these cases, the interaction with the surrounding particles provides sufficient nonlinearity to ensure good ergodicity.

Let us illustrate the effect of approximate mode conservation by a simple example. We model a two–dimensional ring polymer as a chain of 16 beads with mass m. Between each monomer, there is a purely repulsive Lennard–Jones potential

$$U_{LJ}(r) = \begin{cases} 4\varepsilon \left[\left(\frac{\sigma}{r}\right)^{12} - \left(\frac{\sigma}{r}\right)^{6} + \frac{1}{4} \right] & r \leq 2^{1/6}\sigma \\ 0 & r \geq 2^{1/6}\sigma \end{cases} \tag{13}$$

to model the excluded volume interaction. This potential defines the unit system via setting the mass scale m, the length scale σ, and the energy scale ε to unity, such that time is measured in units of $\tau = (m\sigma^2/\varepsilon)^{1/2}$. Bonded monomers are connected along the chain via a FENE backbone potential

$$U_{ch}(r) = -\frac{k}{2} R_0^2 \ln\left(1 - \frac{r^2}{R_0^2}\right), \tag{14}$$

which for small distances behaves like a harmonic spring, while diverging for $r \to R_0$. Parameters which have proved rather useful are

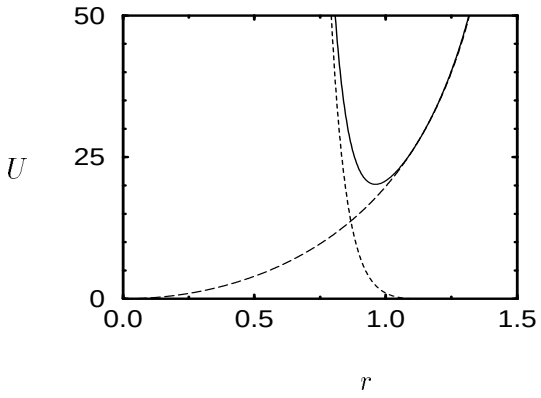

Figure 1: The total potential between two bonded monomers, resulting from the repulsive part U_{LJ} and the attractive part U_{ch}. Energies are in units of ε, distances in units of σ.

$k\sigma^2/\varepsilon = 30$, $R_0/\sigma = 1.5$. They have also been used in the simulation of melts, and are based on the following considerations: one would like to make k rather large and R_0 small, in order to introduce a high energy barrier for self–crossing (this is particularly important in three dimensions). However if k is too large, the interaction between two monomers which are attached becomes very stiff resulting in high frequency modes which can only be integrated accurately with a very small time step. The parameters given are optimized with respect to both properties [31]. The total bond potential is shown in Fig. 1.

Figure 2 shows results of the time development of the ring polymer analog of the end–to–end distance. First the system is run at temperature $T = 1.0\varepsilon/k_B$ with stochastic dynamics based on the Verlet algorithm (details see below), using a time step $h = 0.01\tau$ and a friction constant $\zeta = 0.5\varepsilon\tau/\sigma^2$, which are also typical values for melt simulations. [2] At time $t = 10\,000\tau$ the coupling to the heat bath is turned off ($\zeta = 0$) and the system is run microcanonically. While the fluctuations of R^2 are quite efficiently sampled for nonzero ζ, it varies on a much slower time scale for $\zeta = 0$.

At this point, it is necessary to explain the details of the simulation algorithms. Let us start with the case of purely microcanonical MD. The equations of motion for positions $\vec{r}_i$ and momenta $\vec{p}_i$ are

$$\frac{d}{dt}\vec{r}_i = \vec{p}_i/m_i \qquad\qquad \frac{d}{dt}\vec{p}_i = \vec{F}_i. \tag{15}$$

[2] Tests have shown that when coupled to a heat bath, a melt simulation remains stable even for h as large as 0.0135τ.

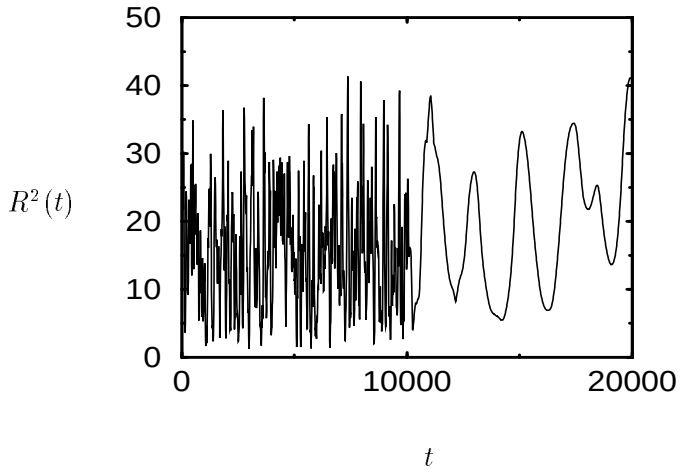

Figure 2: Time development of R^2 with $\vec{R} = \vec{r}_{N/2} - \vec{r}_0$ of a 16–monomer ring polymer. For $0 \leq t \leq 10\,000\tau$ the system is coupled to a heat bath via friction and noise, while for $t > 10\,000\tau$ the chain is run without such a coupling.

In recent years, it has become clear that the Verlet algorithm is a particularly well–suited differential equation solver for Hamiltonian equations of motion, as given above [39]. This is because it is time–reversal symmetric and conserves the phase–space volume, just as the real dynamics does. A systematic drift in, say, the total energy can therefore not occur, since this would mark the two directions of time as not equivalent. Hence, the algorithm is exceptionally stable, allowing for rather large time steps.

A particularly straightforward way to see this is provided by the Liouville operator formalism, where for simplicity we consider one coordinate x with corresponding momentum p, such that the actual trajectory is given by $\hat{x}(t)$, $\hat{p}(t)$, starting at time $t = 0$ at $x = x_0$, $p = p_0$. The corresponding phase–space density is then

$$\delta(x - \hat{x}(t))\delta(p - \hat{p}(t)) = \exp(-i\hat{L}t)\delta(x - x_0)\delta(p - p_0), \qquad (16)$$

where the Liouville operator is given by

$$-i\hat{L} = -i\hat{L}_x - i\hat{L}_p = -\frac{p}{m}\frac{\partial}{\partial x} - F(x)\frac{\partial}{\partial p}. \qquad (17)$$

Since $\hat{L}$ is self–adjoint,

$$\int dx \int dp \quad f^\star(\hat{L}g) \quad = \quad \int dx \int dp \quad (\hat{L}f)^\star g, \qquad (18)$$

the time evolution operator $\exp(-i\hat{L}t)$ is unitary, which shows directly both phase–space volume conservation as well as time–reversal symmetry. The Verlet algorithm replaces this, for a small time step h, by

$$\hat{S}(h) = \exp(-i\hat{L}_p h/2)\exp(-i\hat{L}_x h)\exp(-i\hat{L}_p h/2), \qquad (19)$$

which is manifestly time–reversal symmetric, and unitary, corresponding to the velocity–Verlet updating scheme:

$$x(t+h) = x(t) + h\frac{p(t)}{m} + \frac{h^2}{2m}F\left(x(t)\right) \qquad (20)$$

$$p(t+h) = p(t) + \frac{h}{2}\left[F\left(x(t)\right) + F\left(x(t+h)\right)\right]. \qquad (21)$$

This is the simplest algorithm which is "symplectic", i. e. has the desired properties of time–reversal symmetry and phase–space volume conservation (for each conjugate pair of coordinate and momentum separately). Higher–order symplectic schemes have been constructed on the basis of the same formalism [40]. However, although such an algorithm would permit a larger time step, it would also need several force calculations per time step, and is therefore not considered very useful for MD applications.

Improved stability (i. e. even larger possible time steps) is obtained if one couples the system via friction and noise to a heat bath, i. e. simulates a Langevin equation in a "stochastic dynamics" simulation [41]

$$\dot{x} = p/m \qquad\qquad \dot{p} = F - \zeta p/m + f. \qquad (22)$$

Here, we consider again for simplicity only one degree of freedom, and have introduced a parameter ζ, which is the friction constant which controls how fast the system relaxes into equilibrium — the simulation scheme actually produces states which are distributed according to the canonical ensemble. The temperature results as the ratio of noise strength to friction, via the fluctuation–dissipation theorem: The stochastic force f is a random variable satisfying $\langle f\rangle = 0$, $\langle f(t)f(t')\rangle = 2\zeta k_B T\delta(t-t')$. For more information on Langevin equations, and the corresponding Fokker–Planck equation, see e. g. Ref. [42].

A possible numerical implementation starts from the observation that in the limit $\zeta = 0$ the Langevin simulation reduces to standard microcanonical MD, and that hence one should use the Verlet algorithm also in the "noisy" case. One simply replaces the term Fh,

which is the displacement in momentum space in the microcanonical case, by

$$\Delta p = Fh - \zeta \frac{p}{m} h + \sqrt{2\zeta k_B T h}\, r, \tag{23}$$

where r is a random number with $\langle r \rangle = 0$, $\langle r^2 \rangle = 1$. The prefactor of the stochastic term is chosen such that the mean square stochastic momentum displacement has just the value prescribed by the fluctuation–dissipation theorem. It should be pointed out that the details of the distribution function of r do not matter, as long as the first two moments are zero and one, respectively, and the higher moments exist. This is a straightforward consequence of the Central Limit Theorem [43]. Thus, for simplicity, one should use uniform random numbers.

The reason why this algorithm is even more stable than simple microcanonical MD with the Verlet algorithm is that the stochastic dynamics *thermostats every degree of freedom individually.* Loosely speaking, the noise will "heat up" particles which are "too cold", while the friction will "cool down" particles which are "too hot" and hence would have a tendency to cause instabilities, due to too inaccurate simulation of collision–like processes. This is in marked contrast to the Nose–Hoover thermostat [44], in which only *the overall system* is thermostatted, without additional stability.

Let us now compare the method to other simulation approaches. The "big competitor" is, of course, Monte Carlo (MC) simulations. MC methods are amenable to a number of tricks, which, in many cases, allow for a more efficient sampling of *static* properties. To mention just a few, one can try to "shortcut" the slow physical dynamics by accelerated simulation schemes (in the case of single self–avoiding walks, the pivot algorithm is a typical example; see the contribution of Sokal in this volume and in Ref. [7]). Moreover, there are several reweighting schemes available (umbrella sampling, simulated tempering, multiple Markov chains, etc. [8, 9]), which are, in part, also covered in this volume. However, for MC to also obtain realistic dynamic information, one has to follow the slow physical path. In this case MC is no longer generally superior to MD, particularly for simulations in the continuum. MC codes tend to be slightly more difficult to vectorize and parallelize than MD programs. Good efficiency of MC algorithms is often only obtained when applied to lattice models; however, in many cases the continuum provides considerable flexibility which is hard to attain on a lattice. In particular, one can easily simulate other ensembles including constant pressure or constant stress following the schemes first proposed by Andersen

[45] and Parrinello and Rahman [46]. Moreover, MC on a lattice with local moves requires sufficient amount of free sites in order to keep the acceptance rate high; i. e. for very dense systems a continuum simulation is usually more efficient. The only way out would be to employ an event–driven scheme on the lattice [47], which is however rather complicated.

Similar comments also hold for the comparison with Brownian Dynamics, in which one simulates the *overdamped* Langevin equation

$$\frac{d}{dt}x = \zeta^{-1}\left(F + f\right) \tag{24}$$

(same meaning of symbols as above). This algorithm is often hampered by large discretization errors, and is in spirit quite similar to a MC simulation. One can also combine Brownian Dynamics with Monte Carlo in the so–called "Force–biased Monte Carlo" scheme, where the Brownian Dynamics step is re–interpreted as a Monte Carlo trial move, and, with certain probability, accepted or rejected in order to satisfy detailed balance [48]. However, there are cases where the physics simply *requires* some variant of MD algorithm, and MC cannot describe the phenomena. Loosely speaking, this always occurs whenever *momenta* are important; this is usually the case whenever *hydrodynamics* (i. e. momentum transport) plays a role. An important case is the dynamics of dilute polymer solutions, where hydrodynamic interactions dominate the Brownian motion of the polymer chains: The fast momentum transport mediated by the solvent particles introduces dynamic correlations into the monomers' stochastic displacements, such that one basic assumption of the Rouse model, Eqn. 6, does not hold. Instead, the pertinent model is a modified Rouse model which includes hydrodynamics, the Zimm model [2, 30], which will be described below. In this case, it turns out that even stochastic dynamics alters the dynamics so strongly that it cannot be used to obtain dynamical data.

A last important point concerning simulation methods is, of course, the optimization of the programs. For MD the most time–consuming part is the force calculation. We found it very efficient to use a standard Verlet table, which stores the particle pairs within the interaction range r_c, plus an additional safety margin r_s. This table is reconstructed as soon as a particle has moved more than $r_s/2$, and for this reconstruction we first decompose the system into sub–cells with linear size $\geq r_c + r_s$, such that only the neighboring cells have to be searched and the algorithm scales linearly with the system size. It is possible to set up the table in such a way that the procedure

can be completely vectorized; for more details and a variant of the approach see Refs. [49, 50]. Meanwhile, the scheme has also been quite efficiently parallelized using a geometric decomposition.

3 Zimm model, failure of stochastic dynamics for dilute solutions, and long–range interactions

As already mentioned in the previous section, the momentum transfer through the solvent introduces correlations into the stochastic displacements. The standard theory [2] describes this effect via modeling the momentum transport through the solvent by low–Reynolds number hydrodynamics of an incompressible fluid, i. e. the Navier–Stokes equation for the solvent flow field $\vec{u}$

$$\frac{\partial}{\partial t}\vec{u} = \frac{\eta}{\rho}\Delta\vec{u}, \tag{25}$$

where η is the solvent viscosity and ρ the mass density. The parameter η/ρ, the so–called kinematic viscosity $\eta_{\rm kin}$, has the dimension of a diffusion constant; from the formal analogy of Eqn. 25 to the standard diffusion equation it is obvious that the momentum propagates diffusively with a "diffusion constant" $\eta_{\rm kin}$. For an almost incompressible fluid this mechanism is much faster than the monomer motion (i. e. $\eta_{\rm kin} \gg D_0$). One can therefore still describe the polymer motion via stochastic hops whose correlations are determined just by the instantaneous monomer positions.

Instead of Eqn. 2 one now has

$$\vec{r}_i(t+h) = \vec{r}_i(t) + \sum_j \overleftrightarrow{\mu}_{ij}\ \vec{F}_j h + \vec{\rho}_i, \tag{26}$$

with

$$\langle\vec{\rho}_i\rangle = 0 \tag{27}$$

and

$$\langle\vec{\rho}_i \otimes \vec{\rho}_j\rangle = 2\ \overleftrightarrow{D}_{ij}\ h, \tag{28}$$

where diffusion tensor $\overleftrightarrow{D}_{ij}$ and mobility tensor $\overleftrightarrow{\mu}_{ij}$ are related via $\overleftrightarrow{D}_{ij} = k_B T\ \overleftrightarrow{\mu}_{ij}$, while the Oseen tensor

$$\overleftrightarrow{\mu}_{ij} = \zeta^{-1}\delta_{ij}\ \overleftrightarrow{1} + (1-\delta_{ij})\frac{1}{8\pi\eta r_{ij}}\left(\overleftrightarrow{1} + \frac{\vec{r}_{ij}\otimes\vec{r}_{ij}}{r_{ij}^2}\right) \tag{29}$$

is obtained from the solvent flow field at $\vec{r}_i$ induced by a point force at $\vec{r}_j$.

Following the same reasoning as in the Rouse case to obtain the center–of–mass diffusion constant, one finds the Kirkwood formula

$$D = \frac{D_0}{N} + \frac{k_B T}{6\pi\eta} \left\langle \frac{1}{R_H} \right\rangle, \tag{30}$$

where the hydrodynamic radius of the chain is given by

$$\left\langle \frac{1}{R_H} \right\rangle = \frac{1}{N^2} \sum_{i \neq j} \left\langle \frac{1}{r_{ij}} \right\rangle. \tag{31}$$

Strictly speaking, this formula holds only in the short–time limit of Eqn. 26: The deterministic force contribution to the center–of–mass displacement is now $N^{-1} \sum_{ij} \overleftrightarrow{\mu}_{ij} \vec{F}_j h$, which, in contrast to the Rouse case, does not vanish exactly. However, this term scales only linearly with h, while the stochastic contribution is proportional to $\sqrt{h}$. Hence, for short times this latter part dominates and results in Eqn. 30. The difference between the short–time and long–time diffusion constant is rather small, and the important result is that the diffusion constant now is inversely proportional to the hydrodynamic radius R_H, which is just another measure of the chain dimension. Hence, $D \propto R_G^{-1}$ (note however that there are very strong corrections to scaling), and, in strict analogy to the Rouse case, $z = 3$. This means that all the dynamic scaling laws which have been derived in the previous section hold, but with a dynamic exponent which is smaller due to the hydrodynamic correlations which, on average, speed up the motion of the chain. For example, the subdiffusive behavior of the mean square displacement is now governed by a $t^{2/3}$ law irrespective of chain statistics, while in the Rouse case one has $t^{1/2}$ or $t^{0.54}$ for random walks and self–avoiding walks, respectively.

It is important to note that a simulation which takes both the monomers as well as the solvent particles explicitly into account and also uses stochastic dynamics for every particle cannot describe the hydrodynamic correlations properly. This is immediately evident from the fact that the stochastic dynamics destroys the global momentum conservation, which is the basis for hydrodynamic behavior. Usual Newtonian dynamics for the particle velocities $\vec{u}_i$,

$$\frac{d}{dt}\vec{u}_i = \vec{F}_i/m, \tag{32}$$

directly leads, via coarse–graining, to the Navier–Stokes equation for the velocity flow field $\vec{u}$,

$$\frac{\partial}{\partial t}\vec{u} = \frac{\eta}{\rho}\Delta\vec{u}, \tag{33}$$

and its Oseen type Green's function (in Fourier space),

$$\overleftrightarrow{D} = \frac{1}{(2\pi)^3}\frac{k_B T}{\eta}\int d^3\vec{k}\frac{1-\hat{k}\otimes\hat{k}}{k^2}\exp(i\vec{k}\cdot\vec{r}). \tag{34}$$

Conversely, Langevin dynamics,

$$\frac{d}{dt}\vec{u}_i = \vec{F}_i/m - (\zeta/m)\,\vec{u}_i + \vec{f}_i/m, \tag{35}$$

induces a modified Navier–Stokes equation

$$\frac{\partial}{\partial t}\vec{u} = \frac{\eta}{\rho}\Delta\,\vec{u} - \frac{\zeta}{m}\vec{u}. \tag{36}$$

The frictional term survives the coarse–graining, while the random term averages out. Hence, the original Laplacian is replaced:

$$\Delta \to \Delta - \frac{\rho\zeta}{\eta m} = \Delta - \kappa^2, \tag{37}$$

and the k^2 in the diffusion tensor is replaced by $k^2 + \kappa^2$. Therefore, the hydrodynamic interaction is screened on a characteristic length scale

$$l_0 = \kappa^{-1} = \sqrt{\frac{m\eta}{\rho\zeta}}, \tag{38}$$

in close analogy to electrostatic screening. However, this means that the most important property of the hydrodynamic interaction, its long–range nature, is lost. The intuitive picture of this mechanism is that collisions from particle to particle do not propagate arbitrarily far, but rather are dampened out by the friction and noise, such that after a certain number of events, described by the length scale l_0, the memory of the original momentum is lost. A more formal derivation of this result is found in Ref. [51].

If one carries out a simulation (i. e., studies Brownian motion in an explicit bath of solvent particles), the MD algorithm has, of course, only to deal with short–range interactions. However, the *data analysis* is severely afflicted by the long–range character of the hydrodynamic interaction. Quite generally, the problem about long–range

interactions is that the simulation box is practically always too small to accomodate them by just the "minimum image convention", which takes into account only the interactions within the box itself, and the immediately neighboring periodic images. Rather, one has to sum up the interactions with the infinitely many periodic images. This is usually done by the Ewald summation method [52], which splits the interaction up into a first part, which decays quickly and is summed up in real space, and a second part, which decays slowly but varies smoothly and can hence be summed up efficiently in Fourier space. Such an efficient algorithm is extremely important for the simulation of charged systems [13, 14], but also for the analysis of dynamic simulation data of a single chain in solution Ewald sums have proven extremely useful. In order to take the long–range nature of the hydrodynamic interaction into account, one has to replace the Oseen tensor by its Ewald sum analogue, the formula of which has been given in Ref. [53]. This redefines the hydrodynamic radius, which then becomes an L–dependent effective $R_H(L)$, where L is the linear system size. Since the periodic images effectively increase the chain size, and since the $1/r$ behavior of the Oseen tensor introduces a $1/L$ finite size effect, one has, in leading order [4],

$$\left\langle R_H^{-1} \right\rangle_L = \left\langle R_H^{-1} \right\rangle_{L=\infty} - \text{const.} R_G/L. \tag{39}$$

As will be demonstrated in the following section, this finite size correction is extremely large for systems which can be simulated today, since it is simply impossible to make L orders of magnitude larger than R_G. Even for the particles of a simple fluid this finite size effect of the diffusion constant can be observed, although it is of course much weaker than for a polymer chain. It was shown in Ref. [4] that the data both for solvent particles as well as for the polymer chain are in quantitative agreement with the hydrodynamic theory, with essentially no adjustable parameters.

4 A single chain in a bath of solvent particles

In this section, we briefly summarize the main results of an MD simulation designed to test the predictions of the Zimm model as carefully as possible. A detailed account has been given in Ref. [4], and hence we restrict ourselves only to the main points.

A single chain of up to $N = 60$ monomers was simulated in a bath of up to 7940 solvent particles. To model the excluded volume interactions, the same repulsive Lennard–Jones potential, Eqn. 13, is

introduced between all particles. Since this potential is the same for all particles, this corresponds to an ideal good solvent. The chain structure corresponds to a self–avoiding walk. The temperature $T = 1.2\varepsilon/k_B$, and the fluid density was chosen rather high ($\rho\sigma^3 = 0.864$), in order to approximate the ideal of incompressible flow as closely as possible. The system size was $L = 21\sigma$, and self–overlap effects in the static structure were not observed ($R_G/L \approx 0.2$). The FENE potential parameters were slightly different from those for melt simulations ($k\sigma^2/\varepsilon = 7$, $R_0 = 2\sigma$), and the monomer mass was twice the solvent particle mass. The exact choice of these parameters is of technical relevance but not important for the main results. While stochastic dynamics was used to generate starting states, the dynamics was analyzed from microcanonical runs.

The most important result is that the Zimm prediction $z = 3$ is verified. Figure 3, showing the scaling of the dynamic structure factor for $N = 60$, demonstrates this very clearly. However, when one tries to test the Kirkwood prediction for the diffusion constant, Eqn. 30, finite size effects resulting from the long–range nature of the hydrodynamic interaction show up very clearly. The actual diffusion constant is obtained from the mean square displacement of the center of mass, while the solvent viscosity is calculated via Green–Kubo integration of the time autocorrelation function of the off–diagonal elements of the pressure tensor (see, e. g., Ref. [54]). Moreover, the hydrodynamic radius is obtained via direct averaging of r_{ij}^{-1} as a purely static quantity, and D_0 is estimated via the diffusion constant of the solvent particles. The naive comparison fails completely, the actual diffusion being much slower than the naive Kirkwood prediction. However, when one takes into account the periodic images, i. e. replaces R_H by its Ewald–sum corrected value, the agreement between theory and simulation is nearly perfect. Figure 4 demonstrates that the finite size effect is extremely large. A system which would be large enough to suppress the finite size effect down to 10% would have to contain 3×10^5 solvent particles for the shortest chain $N = 30$!

A similar analysis can be also be done for the generalization of the Kirkwood formula to finite wavenumbers. As Akcasu *et al.* [55–57] have shown, the Zimm dynamics, Eqn. 26, results in an initial decay rate of the dynamic structure factor

$$-\frac{d}{dt}\frac{S(k,t)}{S(k,0)}\bigg|_{t=0} = k^2 D(k) = \frac{\sum_{ij}\left\langle \vec{k}\cdot \overleftrightarrow{D}_{ij}\cdot\vec{k}\exp(i\vec{k}\cdot\vec{r}_{ij})\right\rangle}{\sum_{ij}\left\langle \exp(i\vec{k}\cdot\vec{r}_{ij})\right\rangle}. \qquad (40)$$

This defines a k–dependent diffusion constant $D(k)$, which, in the

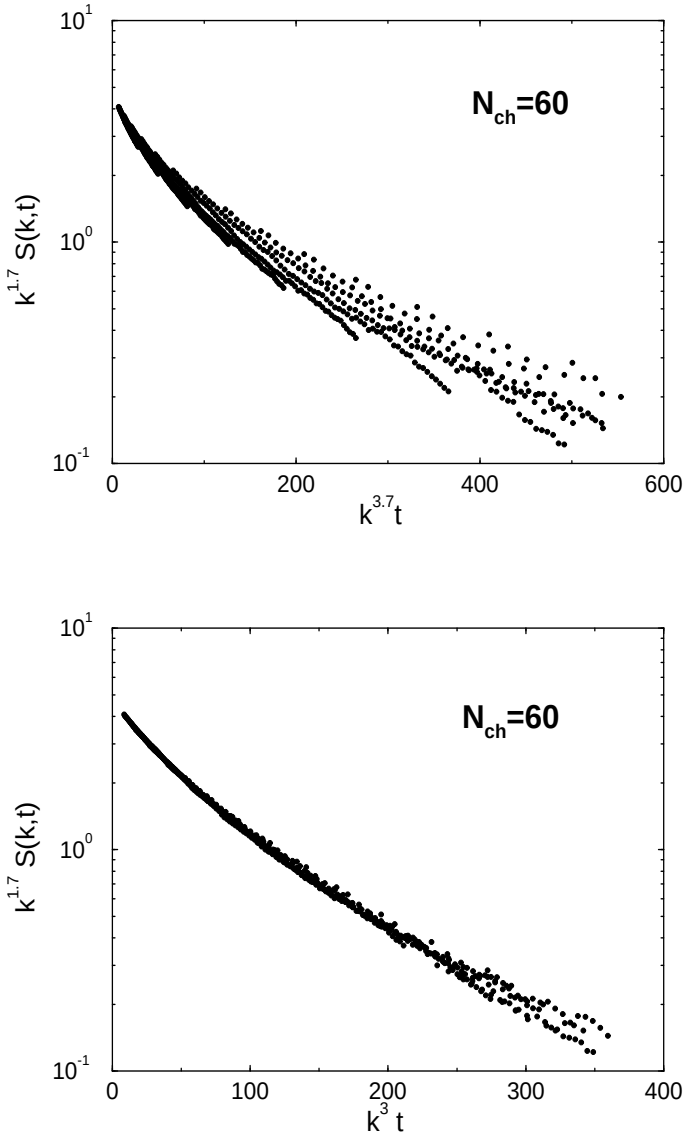

Figure 3: The dynamic structure factor of the $N = 60$ chain, in the scaling regime $0.7 \leq k \leq 3$ and $20 \leq t \leq 80$, plotted in the scaling form $k^{1/\nu} S(k,t)$ vs. $k^z t$, using $z = 2 + 1/\nu = 3.7$ (Rouse scaling) in the upper plot, and $z = 3$ (Zimm scaling) in the lower one.

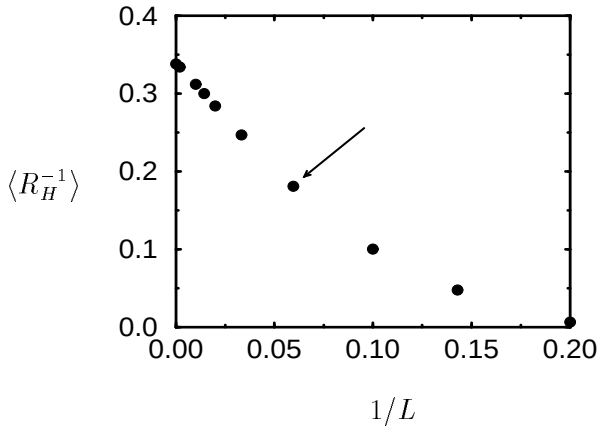

Figure 4: The effective inverse hydrodynamic radius of the $N = 30$ chain, as a function of inverse linear box size, L^{-1}. These data were obtained by putting the configurations of the chain into virtual boxes of size L, and evaluating the Ewald sum average for R_H in each box. The condition of the actual simulation is indicated by an arrow.

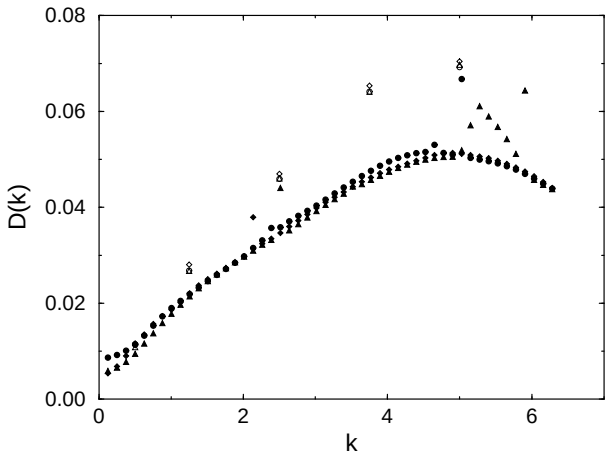

Figure 5: The k–dependent diffusion constant $D(k)$, as defined in Eqn. 40. Full symbols: Upper bound on $D(k)$, obtained from the actual dynamics. Open symbols: Evaluation of the rhs of Eqn. 40, using the Ewald sum for $\overleftrightarrow{D}_{ij}$. Data for various chain lengths are shown: $N = 30$ (circles), $N = 40$ (triangles), and $N = 60$ (diamonds).

limit $k \to 0$, reduces to the center–of–mass diffusion constant. In the same limit, the right hand side reduces to the Kirkwood formula for D_{CM}. The comparison is shown in Fig. 5. One sees that the dynamics data, while in good agreement with the static prediction for $k \to 0$, differ considerably for larger k from the Akcasu prediction. We believe that this is due to more complex dynamics, which cannot be described by simple hydrodynamics, since the length scales are too close to the microscopic ones (note that the typical interparticle distance is of the order of 1, in our units). For a more detailed discussion, see Ref. [4].

5 Entangled melts

In a melt of identical chains the motion of a monomer is, similar to solutions, the result of many complex interactions. The connectivity of the chain plays the same role as before, as a monomer is coupled to its chemical neighbors. The structure of the "solvent", however, is much more complicated, as it consists of other polymer chains rather than small solvent particles. This has many drastic consequences. A fortunate one is that hydrodynamic interactions can be neglected for the study of the monomer motion. The chains strongly interpenetrate and screen the excluded volume interaction. Thus one recovers the random walk exponents for the static properties, e. g.

$$\langle R^2(N) \rangle \propto N. \tag{41}$$

For the dynamics the situation is more complicated. The motion of the monomers is a result of a complicated interplay of collisions and (temporary) constraints. Beyond the connectivity of the monomers under consideration as well as all the other collision partners, the chain topology should play a dominant role. However, as it turns out experimentally, for short chains all these correlations in the forces acting on the monomers average out to a thermal noise which fluctuates very fast compared to the characteristic time for a monomer to diffuse its own diameter. Hence the Rouse model provides a very good description of the dynamics of short polymer chains in a melt of other similar chains. This is an experimental justification of this model rather than a derivation from first principles. It is (probably) impossible to prove the picture, and the Mori–Zwanzig projection operator formalism, which has been applied to the dynamics of polymer melts in the work by Hess [58] and Schweizer [59–62], should be viewed mainly as the proper mathematical language which allows

one to express the physical assumptions as approximations to the full many–body dynamics. However, a rigorous justification of these approximations is not available.

For such melts one finds for the diffusion constant, the viscosity, and the longest relaxation time, respectively, the Rouse scaling laws

$$D = \frac{k_B T}{\zeta N} \tag{42}$$

$$\eta \propto N \tag{43}$$

$$\tau_R \propto N^2. \tag{44}$$

While the center of mass is expected to follow a standard diffusion behavior, one finds for the monomers

$$g_1(t) = \left\langle \left(\vec{r}_i(t) - \vec{r}_i(0)\right)^2 \right\rangle \propto \begin{cases} t^{1/2} & \tau_0 < t < \tau_R \\ t^1 & \tau_R < t \end{cases} . \tag{45}$$

Here τ_0 is the microscopic time, which characterizes the onset of the chain constraints. For intermediate times $g_1(t) \propto t^{2/z}$ (Eqn. 10) with $z = 4$, while for large times the free diffusion takes over.

This is observed, with surprisingly small deviations, for all polymers. When the chains become much longer, i. e. when they significantly exceed a characteristic molecular weight M_e (or characteristic number of monomers N_e), the dynamics is dramatically slowed down. The viscosity changes from $\eta \propto N$ to $\eta \propto N^{3.4}$ and the diffusion constant from $D \propto N^{-1}$ to $D \propto N^{-2}$. This characteristic molecular weight, which can, via $d_T = R(N_e) \propto N_e^{1/2}$, also be viewed as a length scale d_T, differs from polymer to polymer, e. g. $M_e \simeq 850$ for polyethylene (PE), and $M_e \simeq 13\,500$ for polystyrene (PS) for $T = 413K$ [63]. M_e turns out to be extremely temperature–dependent. With increasing T the chains coil more strongly (i. e. R^2 decreases), leading to an increased entanglement molecular weight. For example, at $T = 448K$ the entanglement molecular weight of PE is $M_e \simeq 1350$, while for PS $M_e \simeq 18\,000$ at $T = 485K$ [64, 65]. There have been many attempts to describe this dynamics. The most successful so far is the reptation model [2]. For short chains the connectivity is responsible for the screening of the hydrodynamic interactions. The chains must still be free enough to allow for a slowed down but still isotropic Rouse–like motion. As the chain length increases, the topological constraints, formed by the surrounding chains on intermediate time and length scales, live longer than the time which one monomer needs to escape this "cage" via Rouse–like motion. According to this picture, actually originally applied to networks, the chain is forced to move

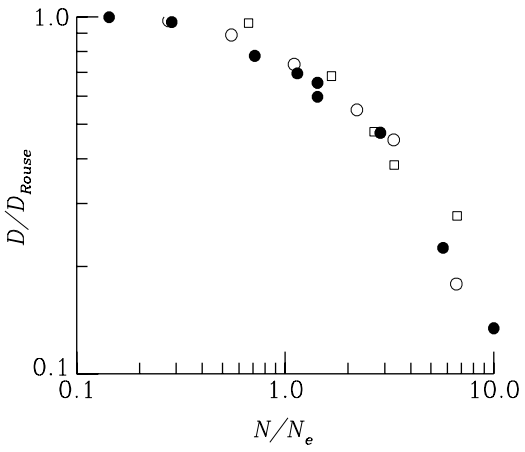

Figure 6: Center–of–mass diffusion constant, normalized by the short–chain Rouse value, as a function of normalized chain length N/N_e. Data taken from this work (closed circles), from MC simulations of the bond fluctuation model at volume fraction 0.5 [33, 34] (open squares), and from hard chain MD simulations by Smith *et al.* [66, 67] at volume fraction 0.45 (open circles).

mainly along its own coarse–grained backbone (one coarse–grained bond corresponds to N_e monomers). This dominance of curvilinear motion leads to a completely different behavior, which is well supported by both simulation and experiment.

The reptation scenario can be described as follows. The chain moves in a diffusive way along its own backbone, while the *curvilinear* diffusion constant D_{curv} is proportional to N^{-1}, due to one–dimensional Rouse motion. The longest relaxation time, the so–called "disengagement time" τ_d, is determined by the requirement that within τ_d the chain has moved its own size. For curvilinear motion, this means however $D_{curv}\tau_d \propto N^2$. Thus one concludes $\tau_d \propto N^3 \propto R_G^6$, i. e. $z = 6$ in the language of the preceding sections. Hence the viscosity in the reptation model also scales as $\eta \propto N^3$ [2], while experimentally one finds $\eta \propto N^{3.4}$, which is commonly viewed as the biggest deficiency of the model, the reasons being still under debate. There are several attempts to include chain end effects (constraint release [58], double reptation [68–72]), as well as alternative models, which do not explicitly take into account the non–crossability of the chains (in particular the mode–mode coupling theory [59–62]). However the most successful so far is the reptation concept. In particular, the experimental finding $D \propto N^{-2}$ is in very good agree-

ment with the reptation model. Since the diffusion constant in real space must satisfy $D\tau_d \propto R_G^2$, $D \propto R_G^{-4} \propto N^{-2}$. Figure 6 shows this crossover from Rouse behavior to reptation, for data taken both from MD as well as MC simulations. Since, however, most experiments can either test only single aspects of the reptation scenario or give rather indirect information, simulations should help to understand the motion of highly entangled polymers. On the other hand, simulations are somewhat limited in the range of chain lengths and the time regime they can study. It is therefore particularly important for simulations to understand the implications of reptation on the intermediate time scales.

For the anisotropic motion of the chain and of the monomers, the reptation model can be described as follows. The topological constraints are pictured in terms of a constraining tube with diameter $d_T \propto N_e^{1/2}$. There are three important crossover times involved: $\tau_e \propto N_e^2$, $\tau_R \propto N^2$, and $\tau_d \propto N^3/N_e$. For $N > N_e$, $\tau_e < \tau_R < \tau_d$, while for $N \simeq N_e$ all three times coincide. For short chains, $N < N_e$, one has Rouse behavior and hence only one time τ_R. The entanglement time τ_e is the Rouse time of a subchain of length N_e; for times smaller than τ_e the monomers do not feel the constraints and hence have Rouse–like motion. The transversal fluctuations of the monomers in the tube have relaxed on the time scale of the Rouse time τ_R, and for times larger than τ_R the motion is completely dominated by the reptation mechanism, i. e. curvilinear diffusion. Finally, after the disengagement time τ_d the motion is simply free diffusion. In terms of the mean square displacement of a monomer, $g_1(t)$, as defined in Eqn. 45, and the mean square displacement of the center of mass,

$$g_3(t) = \left\langle \left(\vec{R}_{CM}(t) - \vec{R}_{CM}(0) \right)^2 \right\rangle , \tag{46}$$

this picture means that for $t < \tau_e$ (disregarding the microscopic time τ_0) one has simply Rouse behavior, i. e. $g_1(t) \propto t^{1/2}$ and $g_3(t) \propto t$. For $t > \tau_R$ the chain moves along its backbone, while fluctuations within the tube give only negligible contributions. For such a type of motion, $g_3(t) \propto t$, with the asymptotic diffusion constant $D \propto N^{-2}$ (this can be shown very easily by considering a "slithering snake" type of motion, where a randomly chosen segment at one of the two ends is removed and attached at the other end), while $g_1(t) \propto t^{1/2}$. This latter behavior is due to the fact that a motion of the chain along the backbone by a distance l corresponds only to a distance of $\propto \sqrt{l}$ in real space, due to the random walk structure of the backbone. Of course, this holds only up to τ_d when the overall diffusion takes

over, such that $g_1(t) \simeq g_3(t) \propto t$ for $t > \tau_d$. Finally, for the crossover regime $\tau_e < t < \tau_R$ we note that the results obtained so far imply

$$g_1(\tau_e) \propto d_T^2 \propto N_e \tag{47}$$

and

$$g_1(\tau_R) \propto g_1(\tau_d) \left(\frac{\tau_R}{\tau_d}\right)^{1/2} \propto N \left(\frac{N_e}{N}\right)^{1/2} \propto (NN_e)^{1/2}, \tag{48}$$

while

$$g_3(\tau_e) \propto \tau_e/N \propto N_e^2/N \tag{49}$$

and

$$g_3(\tau_R) \propto g_3(\tau_d) \left(\frac{\tau_R}{\tau_d}\right) \propto N_e. \tag{50}$$

This is only consistent if in the crossover regime the time behavior is $g_1(t) \propto t^{1/4}$ and $g_3(t) \propto t^{1/2}$.

Let us summarize these findings:

$$g_1(t) \propto \begin{cases} t^{1/2} & \tau_0 < t < \tau_e \propto N_e^2 \\ t^{1/4} & \tau_e < t < \tau_R \propto N^2 \\ t^{1/2} & \tau_R < t < \tau_d \propto N^3/N_e \\ t^1 & \tau_d < t \end{cases} \tag{51}$$

and

$$g_3(t) \propto \begin{cases} t^1 & t < \tau_e \propto N_e^2 \\ t^{1/2} & \tau_e < t < \tau_R \propto N^2 \\ t^1 & \tau_R < t \end{cases} . \tag{52}$$

Due to the detailed sequence of crossovers given by Eqn. 51, $g_1(t)$ is clearly one of the most important quantities to measure. In order to obtain maximum statistics, one would of course average it over all monomers in the system. However, the ends of the chain fluctuate much more strongly than the monomers near the center. Since the theoretical models are for the asymptotic limit of very long chains, it is important to minimize the effect of the chain ends, since the chains which can presently be studied on modern computers are not so highly entangled. Thus, for the remainder of this paper, we average the displacement of the monomers only over the inner monomers, excluding the chain ends. For N even, we usually average over the inner 5 monomers,

$$g_1(t) = \frac{1}{5} \sum_{i=N/2-2}^{N/2+2} \left\langle \left(\vec{r}_i(t) - \vec{r}_i(0)\right)^2 \right\rangle . \tag{53}$$

Other quantities of interest are of course the mean square displacement of the center of mass, $g_3(t)$, whose long–time behavior yields the diffusion constant $D = \lim_{t\to\infty} g_3(t)/(6t)$, and the mean square displacement of a monomer *relative* to the motion of the center of mass,

$$g_2(t) = \frac{1}{5}\sum_{i=N/2-2}^{N/2+2}\left\langle\left(\vec{r}_i(t) - \vec{R}_{CM}(t) - \vec{r}_i(0) + \vec{R}_{CM}(0)\right)^2\right\rangle, \qquad (54)$$

where, for the same reasons as above, we restrict our attention only to the inner monomers. Usually it was assumed [6, 34] that $g_2(t)$ follows the same time behavior as $g_1(t)$ up to τ_R, while for $t > \tau_R$ it was usually assumed to be constant. This corresponds to the sequence $t^{1/2}, t^{1/4}, t^0$. However this leads to an inconsistency: In the long–time regime, the correlation to the original conformation is lost, such that

$$g_2(t\to\infty) = \frac{2}{5}\sum_{i=N/2-2}^{N/2+2}\left\langle\left(\vec{r}_i - \vec{R}_{CM}\right)^2\right\rangle \propto \langle R_G^2\rangle \propto N. \qquad (55)$$

Thus if $g_2(t)$ were already constant at τ_R, this constant should be $g_2(\tau_R) \approx g_1(\tau_R) \propto (NN_e)^{1/2} \ll N$ (cf. Eqn. 48, [6]). Therefore, we conclude that $g_2(t)$ should follow the behavior of $g_1(t)$ up to the disengagement time τ_d, i. e. that a second $t^{1/2}$ regime should occur between τ_R and τ_d. However, so far no indication of this regime has yet been observed. We believe that this is due to a strong "smearing out" of the time behavior, induced by the final crossover to the t^0 regime.

All three displacements allow the definition of a characteristic relaxation time [34] via

$$g_1(\tau_1) = \langle R_G^2\rangle, \qquad (56)$$

$$g_2(\tau_2) = \frac{2}{3}\langle R_G^2\rangle, \qquad (57)$$

$$g_3(\tau_3) = g_2(\tau_3). \qquad (58)$$

This is motivated by the observation that in the ideal Rouse model for noninteracting Gaussian coils all these relaxation times are proportional to each other and the Rouse time τ_R, $\tau_i = C_i\tau_R$, where $C_1 \simeq 0.2410$, $C_2 \simeq 0.2033$, and $C_3 \simeq 0.75$. Taking the ratio of these times to eliminate the unknown quantity τ_R, the Rouse model predicts that $\tau_2/\tau_1 \simeq 0.846$ and $\tau_3/\tau_1 \simeq 3.112$. We compare these ratios

to the results from our MD simulations and from the bond fluctuation simulations of Paul *et al.* [34] below. The reptation prediction is $\tau_1 \propto \tau_2 \propto \tau_3 \propto \tau_d \propto N^3$, where we again have assumed that the final crossover of $g_2(t)$ occurs at τ_d.

In order to observe reptation unambiguously, one should make the ratio N/N_e as large as possible. Firstly, one should try to make N_e small, i. e. simulate the system at high density, since then the tube diameter is expected to be small. Secondly, one should try to simulate long chains. This is however limited by several severe constraints. Large N also means large R_G, and this in turn means a large simulation box. In order to avoid artifacts both in the statics and the dynamics due to the chain seeing itself via the periodic boundary conditions, one chain has to fit nicely into the box. A reasonably large system size is certainly necessary if one attempts to prove or disprove by simulation recent ideas about correlation–hole effects on the long–time dynamics [73]. We view a system size of $L = 7 - 10 R_G$ as the minimum size where one can assume to be rather safe; however, we have usually not been able to reach this goal. Hence, the volume is $L^3 \propto R_G^3 \propto N^{3/2}$, i. e. the number of chains, M, scales as $L^3/N \propto N^{1/2}$. To give an example from our standard MD model, $\langle R_G^2 \rangle = 0.28(N-1)\sigma^2$, i. e. $R_G/\sigma = 3.6$, 5.2, and 7.5 for $N = 50$, 100, and 200, respectively. $L = 7R_G$ would require $M = 270, 410$, and 610 chains, which nowadays could just be done with a big parallel machine. The largest system (with respect to number of monomers) which has been simulated so far contained $M = 120$ chains of length $N = 350$ in a box of $L = 36.7\sigma$, i. e. $L/R_G \approx 3.8$ (in practice, we traded in some "safety" with respect to system size for the ability to go to longer chains at all). For the motion of the internal distances, e. g. the onset of the $t^{1/4}$ regime, this is certainly sufficient, while for the overall diffusion some reservations remain.

Moreover, one has to run the system for several disengagement times, such that the cpu time (of an efficient linear algorithm) scales as $L^3 \tau_d \propto N^{4.5}$ (or $N^{4.9}$, using the experimental viscosity exponent 3.4). This very high power has severely limited the chain length to typically $6 - 8$ N_e. Increasing the chain length by a factor of 2 requires more than a factor of 23 more cpu time, if one wants to cover the entire relaxation spectrum. Thus most simulations give a very precise description for shorter times, while the accuracy significantly decreases for longer times. This is because for smaller times more statistically independent "events" contribute to, say, $g_1(t)$ than for longer times. Fortunately, $g_1(t)$ is a self–averaging quantity, since it refers only to a single chain. Hence, one can improve the statistics by

simply increasing the number of chains, i. e. the relative statistical error is proportional to $M^{-1/2}$. Nevertheless, in order to obtain the full dynamical information, each chain must be observed for a time of several τ_d. The number of statistically independent events per chain contributing to $g_1(m\tau_d)$ $(m > 1)$ can then be crudely estimated as $T_t/(m\tau_d)$, where T_t is the total run length, and prefactors of order unity are ignored. Hence it makes no difference if one improves the statistics via increasing the number of chains, or by increasing the length of the run. However, a larger system size is more amenable to modern massively parallel computers. Note however that this helps to increase the number of chains, but the maximum chain length will still remain limited. Even in the limit of infinitely many available processors, one node still has to treat a sizeable number of monomers in order to keep the communication costs down. Thus the cpu time per processor still scales as τ_d with chain length.

Slightly different considerations apply if one is also interested in quantities which are *not* self–averaging. These are all quantities which are based on *collective* fluctuations of the *overall* system. Typical examples would be the specific heat, the $k \to 0$ limit of the *collective* (i. e. many–chain) structure factor, or the viscosity obtained from equilibrium data via Green–Kubo integration [54], the latter of course being of great interest for studies of polymer dynamics. In this case, the only way to improve the statistics is via longer runs. So far, it has been impossible to obtain reliable viscosity values from equilibrium simulations in the entangled regime. Non–equilibrium MD measurements of the viscosity have been attempted for melts of up to $N = 400$ [26]. A crossover from Rouse–like behavior to reptation was observed for $N \simeq 3N_e$. However, since for the long chains the shear rate was significantly larger than the chain relaxation rate $1/\tau_d$, this simulation was also not able to obtain the asymptotic zero–frequency viscosity. An extrapolation to zero shear must explicitly or implicitly make use of model assumptions on the long–time dynamics, and is moreover severely hampered by chain–stretching effects etc.

The practical conclusion of this discussion is that one needs long runs for medium–sized (with respect to number of monomers) systems. On modern parallel computers with distributed memory there are certainly some lower bounds to the system size. For $MN = 10^5$ we found on a Cray T3D a performance of 0.34 steps per second on one processor. On 64 processors this number is 14 steps per second (i. e. roughly 40 times as fast), while on 256 processors we obtained 45 steps per second (i. e. only 130 times as fast). This is the usual sub–linear speedup due to increased amount of communication over-

Table 1: Simulation details for a melt of M chains of length N at a monomer density $\rho\sigma^3 = 0.85$ and temperature $T = \varepsilon/k_B$, in a simulation cell of linear size L. Data were taken from runs of total time T_t/τ after equilibration. All of the results are for one continuous run for a single ensemble except for $M = 20$ and $N = 50$ which is an average over 5 independent starting states. Results for the mean square radius of gyration $\langle R_G^2 \rangle$, the mean square end–to–end distance $\langle R^2 \rangle$, and the diffusion constant D are given.

M/N	L/σ	T_t/τ	$\langle R_G^2 \rangle/\sigma^2$	$\langle R^2 \rangle/\sigma^2$	$6D\tau/\sigma^2$
200/5	10.6	2.60×10^4	0.9	5.1	8.6×10^{-2}
100/10	10.6	1.30×10^5	2.2	13.0	4.3×10^{-2}
80/25	13.3	2.60×10^5	6.2	37.6	1.4×10^{-2}
50/40	13.3	2.60×10^5	10.4	62.8	7.7×10^{-3}
20/50	10.6	3.38×10^6	13.4	80.8	5.0×10^{-3}
40/50	13.3	1.95×10^5	13.2	79.4	5.8×10^{-3}
100/50	18.1	3.25×10^5	13.3	80.1	5.8×10^{-3}
20/100	13.0	6.50×10^5	27.8	168.4	2.1×10^{-3}
100/100	22.7	3.90×10^5	27.7	167.3	2.1×10^{-3}
100/200	28.7	5.68×10^5	60.4	345.7	5.5×10^{-4}
120/350	36.7	3.84×10^5	93.0	551.7	—

head when one increases the number of processors. While for 256 processors already roughly half of the cpu time is lost in communication overhead, we view the communication losses at 64 processors as still acceptable. This means a minimum number of roughly 1 500 monomers per processor. Note also that even if one is willing to trade in more computing power for a faster throughput, there will finally be a regime where adding yet another processor will actually *decrease* the performance.

In order to further improve on our previous data given in detail in Ref. [6] we carried out a series of new runs for a polymer melt of entangled chains. The system is the same that we have studied in the past, namely a homopolymer melt of linear bead–spring chains at a density $\rho\sigma^3 = 0.85$. Taking advantage of improved algorithms and the lower cost of multi–processor systems, we have studied larger systems for longer times. All of this new data were collected on a Cray 916 (about the speed of an XMP processor) and on a Silicon Graphics Challenger with R4400 processors. The data for the system of 100 chains of length 200 took approximately 85 days of cpu time

on the Cray 916. A summary of our results is presented in Table 1. The data were obtained using a velocity Verlet algorithm to integrate the equations of motion with a time step $h = 0.013\tau$. The friction constant of the stochastic dynamics was $\zeta = 0.5\varepsilon\tau/\sigma^2$. All of the data except for the $M/N = 20/50$ system are the result of one long run for a single system. The data for the 20/50 system are an average over 5 independent starting states in which four were run for a total time $T_t/\tau = 5.2 \times 10^5$ and the fifth run for $T_t/\tau = 1.3 \times 10^6$. To study finite size effects we studied three system sizes, $M = 20$, 40, and 100, for $N = 50$ and two system sizes, $M = 20$ and 100 for $N = 100$. Most of our earlier data were for $M = 20$ [6]. Previously we also studied a system of $M = 100$ chains of 200 but the total length of the run was considerably shorter than presented in Table 1. For the static quantities, like the mean square radius of gyration $\langle R_G^2 \rangle$ and end–to–end distance $\langle R^2 \rangle$, the new results are in very good agreement with the earlier results. There are no detectable finite size effects for the static quantities as the results for $M = 20$ agree very well with those for $M = 100$ for $N = 50$ and 100. For the five independent starting states for $M = 20$ and $N = 50$, the mean values for both $\langle R^2 \rangle$ and $\langle R_G^2 \rangle$ for each sample were all within 1% of the average over the five samples.

The mean square displacements $g_1(t)$ and $g_2(t)$ for the inner 5 monomers of the chain and $g_3(t)$ are shown in Fig. 7 for $N = 100$ and 200. Because of the new, longer runs, this data is of considerably higher quality than data from only a few years ago [6]. While the diffusion constant can be extracted from either $g_1(t)$ or $g_3(t)$ in the limit of long time, our discussion above suggests that $g_3(t)$ reaches the asymptotic limit more rapidly. This can easily be verified by plotting $g_i(t)/t$ vs $\ln t/\tau$ for $i = 1,\ 3$ as shown in Fig. 8. Apart from plots of this type, we also use plots of $g_3(t)/t$ vs. $1/t$ and extrapolate $1/t \to 0$, as done in Fig. 9. The results, which are given in Table 1, are the same within the statistical error for the two methods, provided that the runs are long enough to reach well into the linear regime. The run for the largest system, $N = 350$, is not long enough to reach the asymptotic linear regime and as such we cannot give a reliable estimate of D for this case. We note that these values are higher by about $8 - 20\%$ compared to the values obtained earlier [6], the difference being simply related to the fact that the earlier runs were significantly shorter and on smaller systems than the new ones presented here. Using subsets of our data comparable to the run times presented in Table II of Ref. [6], we find values for D comparable to those presented in our earlier study. Since the total lengths T_t

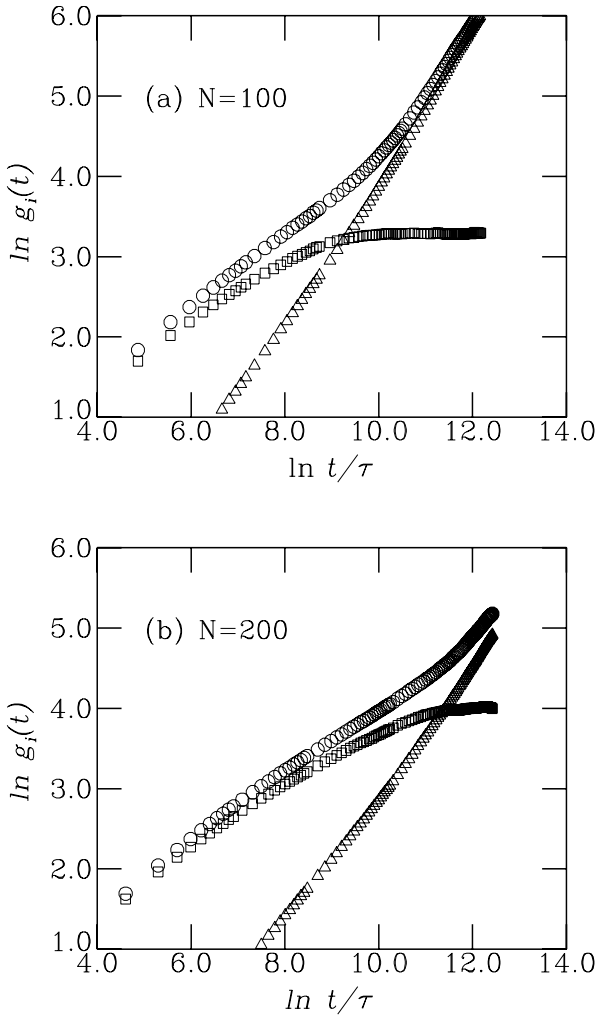

Figure 7: Mean square displacements $g_1(t)$ ($\circ$), $g_2(t)$ ($\square$) for the inner 5 monomers and $g_3(t)$ ($\triangle$) of the center of mass for a system of 100 chains of length $N = 100$ (a) and $N = 200$ (b).

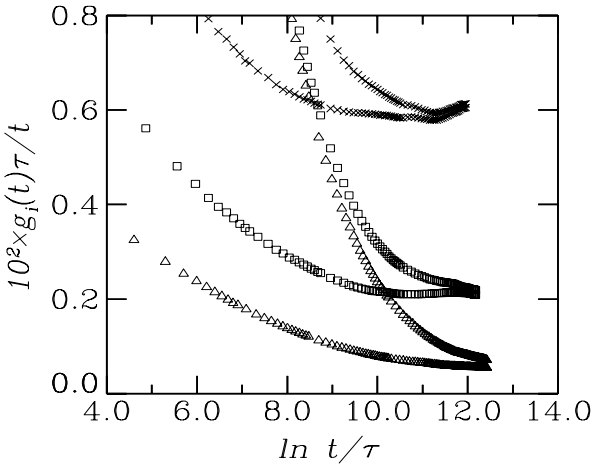

Figure 8: Mean square displacement $g_1(t)/t$ for the inner 5 monomers and $g_3(t)/t$ of the center of mass for a system of 100 chains of length $N = 50$ ($\times$), 100 ($\Box$), and 200 ($\triangle$). The upper curve in each case corresponds to $g_1(t)/t$.

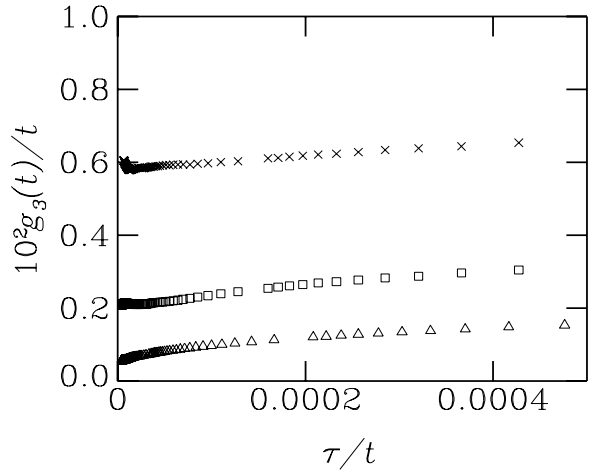

Figure 9: $g_3(t)/t$ plotted as a function of $1/t$, for 100 chains of length $N = 50, 100, 200$. The limiting value for $1/t \to 0$ is $6D$.

of those earlier runs were less than those presented here, the maximum time one could measure $g_3(t)$ was likewise shorter, giving rise to the underestimation of D. Our estimated statistical error in D is about 5% for small N and 10% for large N. However there may be systematic errors, including finite–size effects, which are difficult to estimate. To obtain an estimate of the sample to sample fluctuations in D for small samples, for the system of $M = 20$ chains of length $N = 50$, five independent starting states were run. The results for $6D\tau/\sigma^2 \times 10^3$ varied from 4.8 to 5.3, with an average value of 5.0. All of the runs gave values systematically lower than those found for the larger systems ($M = 40$ and 100). A possible explanation of this finite size effect may be related to the fact that we measure $g_3(t)$ relative to the diffusion of the overall system which arises from the use of the stochastic dynamics algorithm. The motions of the chains are of course correlated, since a monomer must push away its neighbors in order to move. It is well conceivable that for a small number of chains these correlations extend over a significant fraction of the overall system. Hence, a significant part of the chain's own motion might be subtracted, resulting in a systematic underestimation of D. Due to limitations on computer time, multiple runs from different starting states were not made for larger M to check the size of the system to system fluctuation in D. However the difference in the value of D between the $M = 20$ system and the $M = 40, 100$ systems for this case suggests that additional runs for more values of M are needed before we can completely quantitify the systematic error which arises from finite size effects. The fact that within our error bars we find the same value for both $M = 40$ and $M = 100$ suggests that these are likely to be already in the asymptotic large–M regime.

Our MD results for the diffusion constant, normalized by D_{Rouse}, are compared to the bond fluctuation MC simulations of Paul *et al.* [33, 34] for a volume fraction $\Phi = 0.5$ and the hard–chain simulations of Smith *et al.* [66, 67] for $\Phi = 0.45$ in Fig. 6. From this figure it is clear that for small N the diffusion constant scales with N^{-1} as expected. For larger N there is a clear crossover to a slower diffusion. The data is consistent with the reptation prediction that $D \propto N^{-2}$, but is not for sufficiently long chains to prove that the power is 2. Note that all three simulations cover the same range in terms of N/N_e, namely $6 - 7$. At the present time it is still not possible to increase this number by a significant amount.

To test the reptation and mode coupling models of the dynamics, it is important to examine the intermediate time regimes. These are shown in Fig. 10 for $g_1(t)$ for $N = 25, 50, 100, 200,$ and 350. For short

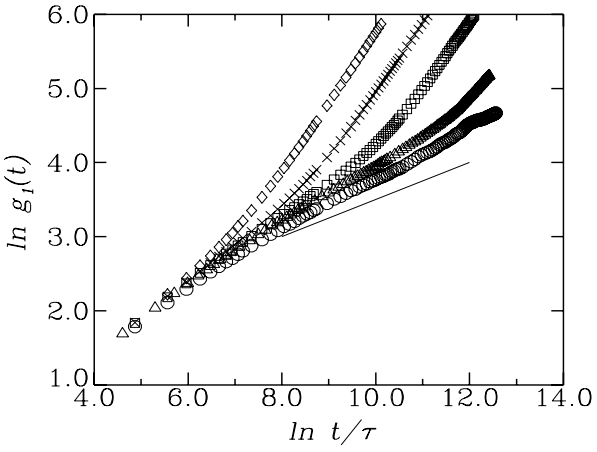

Figure 10: Mean square displacement $g_1(t)$ of the inner 5 monomers for five values of the chain length $N = 25$ ($\diamondsuit$), 50 ($\times$), 100 ($\square$), 200 ($\triangle$) and 350 ($\bigcirc$). The solid line has a slope 1/4.

times, the data for all systems fall on top of each other, as expected from theory. This is because for short times the inner monomers not yet know what the total length of their chain is. With increasing time for $N = 25$, there is a direct crossover from the $t^{1/2}$ regime to free diffusion. However as N increases, there is a definite decrease of the slope of the intermediate regime. Our data give a slope in the intermediate regime of about 0.30 ± 0.03. This slope agrees better with the predictions of the mode coupling theory [59, 60] (9/32) than reptation theory (1/4), though the chain lengths are too short to say for sure that one theory is preferable over the other. As the apparent slope in the intermediate region is clearly decreasing as N increases, it is difficult to determine what the true slope is, in the limit of very large N. Similiar values for the slope of the intermediate time regime have been reported by Skolnick and Kolinski [74], Paul *et al.* [33], Shaffer [75], and Smith *et al.* [66, 67]. The onset of the $t^{1/4}$ regime is identified as τ_e, giving $\tau_e \simeq 1\,800\tau$ for our model. Assuming that τ_e is the relaxation time of a Rouse chain of N_e monomers, one gets $g_1(\tau_e) = 2\langle R_G^2(N_e)\rangle$. This gives $N_e \sim 35$. Since the longest chains which can be fully equilibrated are only of length $N = 200$, the second $t^{1/2}$ regime is expected to be too small to be detected. Reptation theory predicts that it extends from $\tau_R \propto N^2$ to $\tau_d \sim N^3/N_e$, which for $N = 200$ is much less than a decade. For large t, $g_1(t)$ crosses over to diffusion behavior.

Recently Smith *et al.* [66, 67, 76] observed plateaus in $g_1(t)$ versus

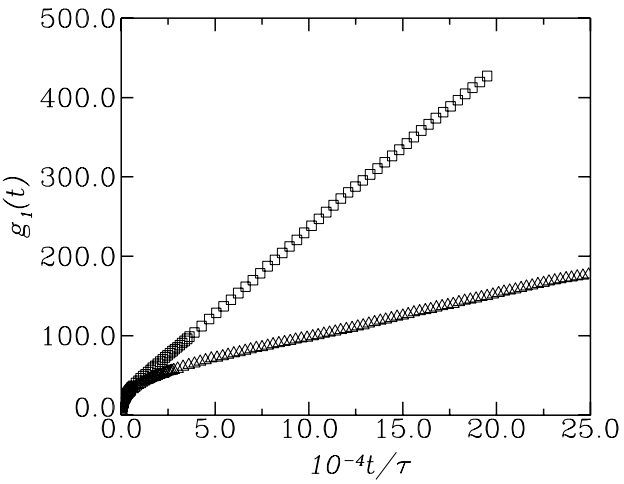

Figure 11: Mean square displacement $g_1(t)$ of the inner 5 monomers for $M = 100$ chains of length $N = 100$ ($\Box$) and 200 ($\triangle$).

t for the inner monomers for their 192–mer fluids. They interpreted these plateaus in terms of intermolecular knots. We looked for evidence of this extra structure in $g_1(t)$ in our new data and found none. In Fig. 11, we re–plot our data from Fig. 10 on a linear–linear scale. The data are presented out to times which are well within the linear late–time regime. From this figure, we see no evidence for extra structure which one could identify as a plateau in $g_1(t)$. This result is in agreement with results of Trautenberg *et al.* [35] who found that they observed similar behavior in their bond–fluctuation simulations of long chains which disappeared or were not reproducible once the system size was increased. Moreover, a direct statistical analysis reveals that the error bar for the data presented in Refs. [66, 67, 76] is expected to be significantly larger than the suggested effect.

Results for the mean square displacement of the center of mass $g_3(t)$ are shown in Fig. 12 for the same five values of N. A slowed down motion for long chains at intermediate times is clearly observable, both in the present MD simulations as well as in previous MC studies [34]. The deviations from Rouse behavior for short times (i. e. $t < \tau_e$ for entangled chains, $t < \tau_R$ for Rouse–like short chains), i. e. a slope $g_3(t) \propto t^{0.8}$ instead of t^1, are found in both MD and MC simulations, and are presently not fully understood.

From data such as that presented in Fig. 7 we can easily determine the relaxation times τ_i. The results are presented in Table 2, where we used the $g_1(t)$ and $g_2(t)$ averaged over the inner 5 monomers to

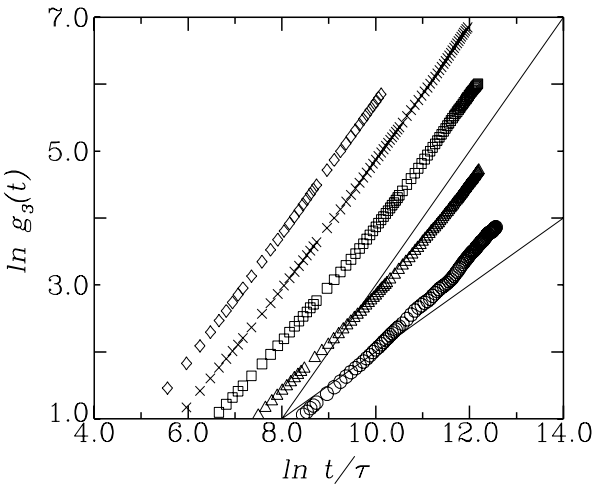

Figure 12: Mean square displacement $g_3(t)$ of the center of mass versus t/τ. The symbols are the same as in Fig. 10. The solid lines have a slope of 1 and 1/2.

Table 2: Simulation results for the three relaxation times τ_i, as defined in Eqs. 56–58.

M/N	τ_1/τ	τ_2/τ_1	τ_3/τ_1	T_t/τ_3
200/5	—	—	—	—
100/10	1.0×10^1	1.1	2.8	4640.0
80/25	1.2×10^2	1.3	2.5	870.0
50/40	3.7×10^2	1.1	2.8	250.0
20/50	7.0×10^2	0.9	3.0	1600.0
40/50	6.4×10^2	1.0	3.0	101.5
100/50	5.9×10^2	1.0	2.9	190.0
20/100	3.9×10^3	0.8	3.3	51.5
100/100	3.3×10^3	0.9	3.3	35.8
100/200	2.7×10^4	0.7	3.3	6.4
120/350	1.7×10^5	0.5	3.0[a]	0.8

[a] The value for τ_3 for $N = 350$ is determined by extrapolation of $g_2(t)$ and $g_3(t)$ and as such is not as reliable as for $N \leq 200$.

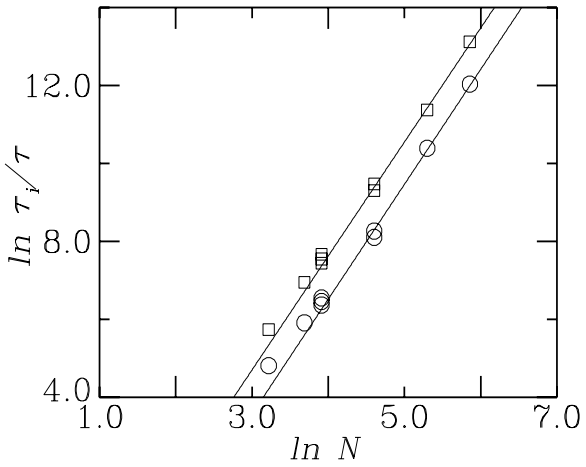

Figure 13: Relaxation time τ_1 ($\square$) and τ_3 ($\bigcirc$) as a function of the chain length N. The lines are best linear least square fits to the data for $50 \leq N \leq 350$. The slope of the solid line is 2.9 for both τ_1 and τ_3.

determine τ_i. In Fig. 13 we present our results for τ_1 and τ_3 as function of N. As seen from the figure, the data are fitted by a power law $\tau_i \propto N^a$, with $a = 2.9 \pm 0.1$. A similar plot for τ_2 gives a slope of 2.6 ± 0.1. The ratios for τ_2/τ_1 and τ_3/τ_1 are consistent with those reported by Paul *et al.* [34] for the bond fluctuation model. The data agree very well with the reptation prediction for τ_1 and τ_3, at least for the limited range of N studied. However N is not large enough to rule out a 3.4 power as observed experimentally. The exponent $a = 2.6$ for τ_2 does not agree very well with the reptation prediction; this is probably due to the very smooth crossover behavior of $g_2(t)$. Larger N are clearly needed to distinguish crossover effects from asymptotic behavior, particulary when examining the largest relaxation times in the system.

As discussed above, in order to obtain full dynamical information, one would like to determine the mean square displacement $g_1(t)$ out to a time of order $10\tau_d$. In order to estimate the quality of the data, it is important to measure the length of the run T_t in terms of the longest relaxation time in the system. We use τ_3 as an estimate of τ_d, since this is always the largest of the three values as seen in Table 2. From these results, we see that for $N \leq 100$, all of the simulations met our desired target of $T_t/\tau_3 > 10$, while the run for $N = 200$ was somewhat less, $T_t/\tau_3 = 6.4$. Thus all of the runs for $N \leq 100$ were of sufficient length to be able to average the mean square displacement

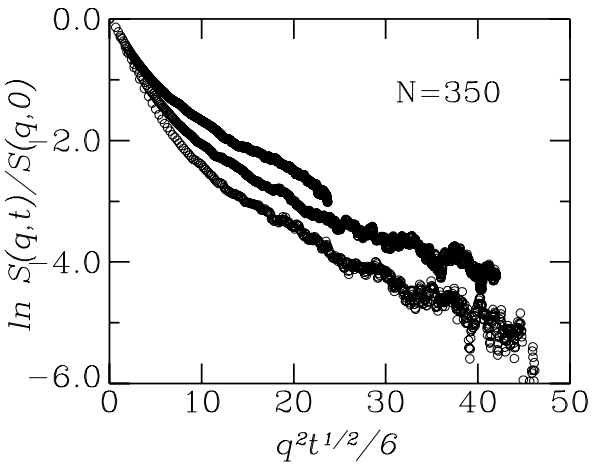

Figure 14: Semilog plot of the normalized coherent single–chain structure factor $S(q,t)/S(q,0)$ as a function of scaled time $q^2t^{1/2}/6$ for $N = 350$. Only the inner $N_s = 50$ monomers have been taken into account. The three curves correspond to different values of $q\sigma = 0.6$, 0.8, and 1.0 (top to bottom). The slowing down for long time is a clear signature of non–Rouse behavior.

of the inner monomers $g_1(t)$ and the center of mass $g_3(t)$ out to a time greater than $10\tau_3$ and thus well into the linear time domain, while the same two quantities for $N = 200$ could only be measured with reasonable accuracy out to about $3\tau_3$. The run for $N = 350$, though very long, was clearly too short to give an accurate estimate of the long time diffusion constant, though it was long enough to examine the intermediate time domain. These results clearly demonstrate the difficulty in going beyond the present limitation of $6 - 7N_e$. The relaxation times simply increase so rapidly that only an increase of N to $10N_e$ would take considerable computational resources, which are available today only on the largest multi–processor platforms.

Figure 14 shows the decay of the single–chain intermediate coherent scattering function $S(q,t)/S(q,0)$, which can be measured by neutron spin echo experiments [77–79]. The slowdown of the monomer motion due to the topological constraints shows also up in this function, however, in a similar fashion as for the mean square displacements, end effects tend to blur the signature of reptation. Hence it is important to go well into the entangled regime ($N = 350$ was chosen for Fig. 14), and again restrict attention only to inner monomers. Hence, only the 50 inner monomers contribute to the scattering function. This is of experimental relevance since one can label the inner

part of the chain by deuteration. The wave numbers q in Fig. 14 have been chosen well within the scaling regime where the static structure factor decays as q^{-2}. In this regime, the Rouse model predicts a decay

$$\frac{S(q,t)}{S(q,0)} = \exp\left(-\text{const.}q^2 t^{1/2}\right), \tag{59}$$

which however in Fig. 14 holds only in the short–time regime $t < \tau_e$. For longer times, the curves split up and exhibit a much slower decay, which is an indication of reptation. For a more detailed discussion, see Ref. [6]. A detailed comparison of the intermediate coherent scattering function for the bond fluctuation model and the double reptation theory of des Cloizeaux [68–72] was recently presented by Wittmer, Paul and Binder [80].

As seen from this brief summary of work on simulations of entangled polymer melts, it is clear that in the past few years there has been considerable progress in the understanding of melt dynamics through MD simulations. The simulations clearly show that the entanglement length is the unique length scale which governs the slowing down of the overall motion of the polymers. However the data are not accurate enough to distinguish between the predictions of the reptation scheme and mode coupling approaches. It should however be kept in mind that the mode coupling theory does *not* take into account the non–crossability of the chains. Applied to polymer networks, where the reptation model originates from, the mode coupling theory necessarily leads to incorrect results [16, 19–21]. To distinguish these models, longer chains are needed. However there is a significant hurdle to overcome to extend the simulations beyond the present limit of $6-7$ entanglement lengths. As seen from the work presented here, increasing the chain length to 10 entanglement lengths is quite cpu intensive. Unfortunately chains of $10N_e$ are not really long enough to settle many of the open questions. To do this, we estimate that chains of at least $20N_e$ are needed, because for shorter chains the power law regime between the $t^{1/4}$ regime and the linear diffusive time regime is simply too short to determine the exponent unambiguously. Chains of this length are also needed to distinguish the reptation prediction for the longest relaxation time, $\tau_d \propto N^3$, from the experimental result, $N^{3.4}$. Using the time estimates for the Cray T3D discussed above, we estimate that about 1 300 cpu hours on 256 processors would be required to run a system of 100 chains of 20 entanglement lengths ($N = 700$) for a time of order τ_3, assuming the N^3 scaling persists for larger N. Further program optimizations on

production machines are expected to give some speedup of roughly a factor of two. Thus, even though there have been significant advances with respect to both hardware performance as well as program development, studies of this type are currently not feasible, as a run of τ_3 is clearly not sufficient to obtain good averaging with only $M = 100$ chains. However, on future parallel machines with significantly increased single–processor performance, the interesting regime might come well into reach. Major breakthroughs in our understanding of polymer dynamics, not only for melts but also for semi–dilute solutions, are expected. Thus it is clear that this is an exciting time for polymer simulations and the future looks encouraging.

References

[1] P. G. de Gennes, *Scaling Concepts in Polymer Physics* (Cornell University Press, Ithaca, 1979).

[2] M. Doi and S. F. Edwards, *The Theory of Polymer Dynamics* (Clarendon Press, Oxford, 1986).

[3] B. Dünweg and K. Kremer, Phys. Rev. Lett. **66**, 2996 (1991).

[4] B. Dünweg and K. Kremer, J. Chem. Phys. **99**, 6983 (1993).

[5] K. Kremer, G. S. Grest, and I. Carmesin, Phys. Rev. Lett. **61**, 566 (1988).

[6] K. Kremer and G. S. Grest, J. Chem. Phys. **92**, 5057 (1990).

[7] *Monte Carlo and Molecular Dynamics Simulations in Polymer Science*, edited by K. Binder (Oxford University Press, New York, 1995).

[8] *Monte Carlo and Molecular Dynamics of Condensed Matter Systems*, edited by K. Binder and G. Ciccotti (Italian Physical Society, Bologna, 1996).

[9] *Computer Simulation in Chemical Physics*, edited by M. P. Allen and D. J. Tildesley (Kluwer Academic Publishers, Dordrecht, 1993).

[10] *Molecular–Dynamics Simulation of Statistical–Mechanical Systems*, edited by G. Ciccotti and W. G. Hoover (North–Holland, Amsterdam, 1986).

[11] M. P. Allen and D. J. Tildesley, *Computer Simulation of Liquids* (Clarendon, Oxford, 1987).

[12] D. C. Rapaport, *The Art of Molecular Dynamics Simulation* (Cambridge University Press, New York, 1995).

[13] M. J. Stevens and K. Kremer, Phys. Rev. Lett. **71**, 2228 (1993).

[14] M. J. Stevens and K. Kremer, J. Chem. Phys. **103**, 1669 (1995).

[15] U. Micka and K. Kremer, 1996, preprint.

[16] E. R. Duering, K. Kremer, and G. S. Grest, Phys. Rev. Lett. **67**, 3531 (1991).

[17] G. S. Grest, K. Kremer, and E. R. Duering, Europhys. Lett. **19**, 195 (1992).

[18] E. R. Duering, K. Kremer, and G. S. Grest, Macromolecules **26**, 3241 (1993).

[19] E. R. Duering, K. Kremer, and G. S. Grest, J. Chem. Phys. **101**, 8169 (1994).

[20] R. Everaers and K. Kremer, Macromolecules **28**, 7291 (1995).

[21] R. Everaers and K. Kremer, 1996, preprint.

[22] G. S. Grest and M. Murat, in Ref. [7].

[23] G. S. Grest, M.-D. Lacasse, K. Kremer, and A. Gupta, 1996, preprint.

[24] C. Pierleoni and J.-P. Ryckaert, Phys. Rev. Lett. **71**, 1724 (1993).

[25] C. Pierleoni and J.-P. Ryckaert, Macromolecules **28**, 5087 (1995).

[26] M. Kröger, Rheology **95 5**, 66 (1995).

[27] P. E. Rouse, J. Chem. Phys. **21**, 1272 (1953).

[28] J. G. Kirkwood and J. Riseman, J. Chem. Phys. **16**, 565 (1948).

[29] J. J. Erpenbeck and J. G. Kirkwood, J. Chem. Phys. **29**, 909 (1958).

[30] B. H. Zimm, J. Chem. Phys. **24**, 269 (1956).

[31] G. Grest and K. Kremer, Phys. Rev. A **33**, 3628 (1986).

[32] K. Kremer and K. Binder, Comp. Phys. Reports **7**, 259 (1988).

[33] W. Paul, K. Binder, D. W. Heermann, and K. Kremer, J. Phys. II (Paris) **1**, 37 (1991).

[34] W. Paul, K. Binder, D. W. Heermann, and K. Kremer, J. Chem. Phys. **95**, 7726 (1991).

[35] H. L. Trautenberg, M. Wittkop, T. Hölzl, and D. Göritz, Phys. Rev. Lett. **76**, 4448 (1996).

[36] H. J. Hilhorst and J. M. Deutch, J. Chem. Phys. **63**, 5153 (1975).

[37] C. Pierleoni and J.-P. Ryckaert, Phys. Rev. Lett. **61**, 2992 (1991).

[38] C. Pierleoni and J.-P. Ryckaert, J. Chem. Phys. **96**, 8539 (1992).

[39] M. Tuckerman, G. J. Martyna, and B. J. Berne, J. Chem. Phys. **97**, 1990 (1992).

[40] H. Yoshida, Phys. Lett. A **150**, 262 (1990).

[41] T. Schneider and E. Stoll, Phys. Rev. **B 17**, 1302 (1978).

[42] H. Risken, *The Fokker–Planck Equation* (Springer, Berlin, 1984).

[43] B. Dünweg and W. Paul, Int. Journ. Mod. Phys. C **2**, 817 (1991).

[44] S. Nose, J. Chem. Phys. **81**, 511 (1984).

[45] H. C. Andersen, J. Chem. Phys. **72**, 2384 (1980).

[46] M. Parrinello and A. Rahman, Phys. Rev. Lett. **45**, 1196 (1980).

[47] A. B. Bortz, M. H. Kalos, and J. L. Lebowitz, J. Comp. Phys. **17**, 10 (1975).

[48] D. Ceperley, M. H. Kalos, and J. L. Lebowitz, Macromolecules **14**, 1472 (1981).

[49] G. S. Grest, B. Dünweg, and K. Kremer, Comp. Phys. Comm. **55**, 269 (1989).

[50] R. Everaers and K. Kremer, Comp. Phys. Comm. **81**, 19 (1994).

[51] B. Dünweg, J. Chem. Phys. **99**, 6977 (1993).

[52] B. R. A. Nijboer and F. W. de Wette, Physica **23**, 309 (1957).

[53] C. W. J. Beenakker, J. Chem. Phys. **85**, 1581 (1986).

[54] J. P. Hansen and I. R. McDonald, *Theory of Simple Liquids* (Academic Press, New York, 1986).

[55] A. Z. Akcasu, M. Benmouna, and C. C. Han, Polymer **21**, 866 (1980).

[56] C. C. Han and A. Z. Akacsu, Macromolecules **14**, 1080 (1981).

[57] M. Benmouna and A. Z. Akcasu, Macromolecules **13**, 409 (1980).

[58] W. Hess, Macromolecules **21**, 2620 (1988).

[59] K. Schweizer, J. Chem. Phys. **91**, 5802 (1989).

[60] K. Schweizer, J. Chem. Phys. **91**, 5822 (1989).

[61] K. Schweizer, J. Non–Cryst. Solids **131–133**, 643 (1991).

[62] K. Schweizer, Physica Scripta **T 49**, 99 (1993).

[63] L. J. Fetters *et al.*, Macromolecules **27**, 4639 (1994).

[64] D. S. Pearson, G. ver Strate, E. von Meerwall, and F. C. Shilling, Macromolecules **20**, 1133 (1987).

[65] M. Antonietti, K. J. Fölsch, and H. Sillescu, Makrom. Chem. **188**, 2317 (1987).

[66] S. W. Smith, C. K. Hall, and B. D. Freeman, Phys. Rev. Lett. **75**, 1316 (1995).

[67] S. W. Smith, C. Hall, and B. D. Freeman, J. Chem. Phys. **104**, 5616 (1996).

[68] J. des Cloizeaux, Europhys. Lett. **5**, 437 (1988).

[69] J. des Cloizeaux, Europhys. Lett. **6**, 475 (1988).

[70] J. des Cloizeaux, Macromolecules **23**, 3992 (1990).

[71] J. des Cloizeaux, Macromolecules **23**, 4678 (1990).

[72] J. des Cloizeaux, Macromolecules **25**, 835 (1992).

[73] A. N. Semenov, Physica A **166**, 263 (1990).

[74] J. Skolnick and A. Kolinski, in *Advances in Chemical Physics*, edited by I. Prigogine and S. A. Rice (Wiley, New York, 1990), Vol. 78, p. 223.

[75] J. S. Shaffer, J. Chem. Phys. **101**, 4205 (1994).

[76] S. W. Smith, C. K. Hall, and B. D. Freeman, Phys. Rev. Lett. **76**, 4449 (1996).

[77] D. Richter, B. Ewen, B. Farago, and T. Wagner, Phys. Rev. Lett. **62**, 2140 (1989).

[78] D. Richter *et al.*, Macromolecules **25**, 6156 (1992).

[79] D. Richter *et al.*, Phys. Rev. Lett. **71**, 4158 (1993).

[80] J. Wittmer, W. Paul, and K. Binder, J. Phys. II (France) **4**, 873 (1994).